Ecotoxicology and Environmental Safety 289 (2025) 117700

Contents lists available at ScienceDirect

Ecotoxicology and Environmental Safety

journal homepage: www.elsevier.com/locate/ecoenv

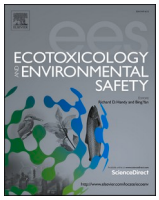

Oxidative degradation of sulfamethazine by manganese oxide supported biochar activated periodate: Effect and mechanism

Shuheng Hu [a], Hao Lu [a,b], Wenyi Xie [b], Shaohua Cao [b], Jiaqi Shi [b,*], Yang Guo [b], Xin Zhu [b], Zimu Xu [a], Han Gao [b,*]

[a] School of Resources and Environmental Engineering, Hefei University of Technology, Hefei, Anhui 230009, China
[b] State Environmental Protection Key Laboratory of Soil Environmental Management and Pollution Control, Nanjing Institute of Environmental Sciences, Ministry of Ecology and Environment of China, Nanjing, Jiangsu, 210042, China

ARTICLE INFO

Edited by: Professor Bing Yan

Keywords:
Biochar
Manganese oxide
Antibiotic
Periodate
Advanced oxidation process

ABSTRACT

In this study, manganese oxide supported biochar (MBC) was used as a catalyst of periodate (PI) for the oxidative degradation of sulfonamide antibiotic sulfamethazine (SMZ). The degradation rate of 10 mg/L SMZ reached 99 % in 60 min in the MBC/PI system, and the optimal condition was pH 3.5, 0.12 g/L of MBC, and 0.17 mM of PI. Combined with quenching experiment and electron paramagnetic resonance (EPR) characterization, it was determined that the reactive oxygen species (ROS) participating in the reaction include iodate radical (IO_3•), singlet oxygen ($^1O_2$), and hydroxyl radical (•OH). ROS, Mn(III) and electron transfer are three crucial SMZ removal mechanisms in MBC activated PI system, and the conversion process of reactive species was deduced. The manganese redox cycles, oxygen-containing functional groups on MBC surface, and BC-O-Mn(II) complex participated in reactive species production. The loading of manganese oxide increases the number of oxygen-containing functional group on the surface of BC, and BC-O-Mn(II) complex formation resulted in the higher catalytic activity compared with BC. Ten SMZ oxidative products and four transformation pathways was identified. This study provided an efficient and practical method to remove sulfonamide antibiotics and revealed its theoretical mechanism.

1. Introduction

With the increase in public's awareness of health protection, the use of antibiotics as therapeutic and preventive drugs for infectious diseases in humans and animals continues to grow (Binh et al., 2018, Zhao et al., 2019). Sulfonamide antibiotic (SA) is one of the most widely used antibiotics. At the beginning of the 21st century, the global use of antibiotics ranged from 1.0×10^5 to 2.0×10^5 tons per year, of which more than 2.0×10^4 tons were used in the case of SA (Baran et al., 2011). SA is more commonly used as veterinary medicine. It was reported that the total use of SA as veterinary antibiotics worldwide was roughly 6.3×10^4 tons in 2010, and was expected to increase by 67 % by 2030 (Van Boeckel et al., 2015). SA existed prevalently in aquatic environment, posing serious threats to marine plants, animals, microorganisms, and human health. Previous studies have shown that antibiotics inhibit the growth of microalgae, affect their pigment synthesis, hinder photosynthesis, and cause oxidative damage (Chen et al., 2020). Li et al. studied the toxic effects of 13 different antibiotics on freshwater algae, and the results showed that most antibiotics were toxic to green algae (Li et al., 2016). The SA accumulated in human body would cause neurological and hematopoietic disorders, genitourinary system and liver damages (Champagne-Jorgensen et al., 2019). Wastewater from the production and use of these antibiotics enters surface and groundwater and accumulates in the human body through various pathways, much of which can be attributed to insufficient treatment in wastewater treatment facilities. Therefore, it is of great practical significance to utilize effective methods to degrade SA and convert it into non-toxic substances.

Advanced oxidation process (AOPs) is a pollutant treatment technology that can produce strong oxidizing free radicals (hydroxyl radical (•OH), superoxide radicals ($O2•^-$), etc.) and has the characteristics of high reaction speed and strong oxidation capacity. Many AOPs, including Fenton, activated persulfate, ozonization, and photocatalytic oxidation, are employed to eliminate organic contaminants like antibiotics (Li et al., 2023a, 2023b). Fenton oxidation process has the advantages of high degradation efficiency and simple operation, but is

* Correspondence to: 8 Jiangwangmiao Street, Nanjing, PR China.
E-mail addresses: sjq@nies.org (J. Shi), gaohan@nies.org (H. Gao).

https://doi.org/10.1016/j.ecoenv.2025.117700
Received 6 November 2024; Received in revised form 26 December 2024; Accepted 5 January 2025
Available online 10 January 2025

limited to acidic condition and produces a large amount of iron-containing sludge, which is difficult to treat (Wang and Zhuan, 2020). Due to the high oxidation potential (E_0=2.08 V), ozone could degrade antibiotics well, and no dangerous by-products form in the process. Its main disadvantage is the need to produce ozone from oxygen, for which electrical discharge is required on the air stream or pure oxygen stream, a step that consumes a lot of energy (Anjali and Shanthakumar, 2019). The photocatalytic oxidation of antibiotics produces pairs of hole electrons (h^+/e^-), and had low external energy consumption. However, it is difficult to achieve uniform radiation on the entire surface of the catalyst in a larger range, and subsequent separation treatment is required to recover the suspended catalyst (Cuerda-Correa et al., 2020). In recent years, a new precursor periodate (PI) with a redox potential of (+1.60 V) has been studied for generating more reactive oxygen species (ROS) to degrade refractory organics (Yang et al., 2022). It has high stability, low cost, easy storage and transportation. In the activation process, new free radicals, such as iodate radical (IO_3•) and periodate radical (IO_4•) are produced, which have short action time and high degradation efficiency on refractory organic matter. PI activation produces fewer by-products, resulting in less secondary water pollution. Therefore, PI was selected in this work to degrade sulfamethazine (SMZ) (Zou et al., 2024).

Due to the low redox potential of PI, it requires to be activated by catalyst for pollutant removal (Long et al., 2021). According to recent research, biochar (BC) is an effective and affordable periodate activator because of its rich pore structure and oxygenated functional groups on the surface (Luo et al., 2023, Qiu et al., 2022). Dai et al. revealed that the electron transfer mechanism dominated the BC activated PI process (Dai et al., 2023). He (He et al., 2022a, 2022b) found that ultrasound could stimulate the sludge BC activated periodate system to produce more •OH and singlet oxygens ($^1O_2$), and enhance the degradation of levofloxacin. However, when BC is used as catalyst alone, its ability to remove pollutants is limited, so it needs to be modified to achieve the best degradation effect (Tan et al., 2015). Manganese oxides (MnO_x) have low biotoxicity and abundant natural reserves (Zhu et al., 2019). MnO_2 has shown excellent catalytic effect on PI. Du et al. revealed experimentally that MnO_2 activated PI well, and Mn(IV)-O-IO_3 complex formed, which further produced $^1O_2$ and IO_3• to oxidize sulfanilamide (Du et al., 2020). Fan et al. suggested that in comparison to BC itself, BC enriched with manganese oxide activated Orange G's persulfate (PS) degradation more effectively (Fan et al., 2019). Therefore, the combined activation of BC and MnO_x on PI to degrade SMZ might be a good choice. Nevertheless, its effect and mechanism are still unrevealed.

Therefore, In this study, MnO_x supported BC (MBC) was prepared by impregnation method, and its ability to remove SMZ, influencing factors and reaction mechanism were investigated. The degradation path of SMZ was revealed. This study provides theoretical and practical basis for solving the SMZ degradation problem scientifically and efficiently, and provides theoretical and experimental support for the application of MBC/PI system in wastewater treatment.

2. Materials and methods

2.1. Chemicals and reagents

SMZ, humic acid (HA), L-histidine (L-His), and sodium pyrophosphate decahydrate (PP) were purchased from Aladdin Reagent Co., LTD (Shanghai, China). Sodium periodate ($NaIO_4$), manganese acetate, and furfuryl alcohol (FFA) were purchased from MackLin reagent Co., LTD. Potassium permanganate ($KMnO_4$), sodium thiosulfate ($Na_2S_2O_3$•5 H_2O), sodium chloride (NaCl), sodium bicarbonate ($NaHCO_3$), sodium dihydrogen phosphate (NaH_2PO_4•2 H_2O), sodium nitrate ($NaNO_3$), sodium sulfatesulfate ($NaSO_4$), methanol (MeOH), dimethylsulphoxide (DMSO), tertiary butyl alcohol (TBA), phenol, and chloroform (CF) were obtained from Sinopharm Chemical Reagent Co., LTD. All chemicals were of analytical grade and all solutions were prepared with ultrapure water (18.25 MΩ cm).

2.2. BC and MBC preparation

The BC was prepared in the following way: the corn stover was washed, crushed to powder, and then was pyrolyzed at 500 °C for 2 h. The resulting powder was washed with deionized water several times and dried through a 100-mesh sieve to make BC.

MBC was prepared as follows: 15.00 g BC and 3.16 g $KMnO_4$ were mixed using 150 mL deionized water with stirring at room temperature, followed by 0.5 h ultrasonic vibration to ensure the sufficient contact between BC and $KMnO_4$. Then, 100 mL of 0.3 M manganese(II) dissolved in acetate solution was added to the BC and $KMnO_4$ mixture with continuous stirring to obtain the suspension. The suspension was heated in a water bath at 80 °C for 30 min, and filtered through 0.22 μm filter to obtain the MBC. The MBC was washed four times using deionized water, and dried at 80 °C for further use (Liang et al., 2017).

2.3. Experimental and analytical methods

The reaction solution contained 0.005 g of biochar, 0.15 mM PI and 10 mg/L SMZ with a total volume of 50 mL. The reaction was carried out at 400 r/min, pH 5.00, and 25°C on a magnetic stirrer. Sample aliquots (1 mL) were withdrawn at the specified time (0 min, 1 min, 2 min, 5 min, 10 min, 30 min, and 60 min) during reaction. The sample were filtered through 0.22 μm aqueous filter, and transfered to a 2 mL brown injection vial. The reaction was terminated by the rapid addition of 20 μL of 1 M $Na_2S_2O_3$ solution. The SMZ was quantified by a high-performance liquid chromatograph (HPLC, Shimadu LC20AD). The intermediates were determined by high-performance liquid chromatography-mass spectrometry (HPLC-MS, Agilent 1100 + TSQ quantum Uitra AM, USA).

2.4. Box-behnken design

Response surface method (RSM) is a comprehensive optimization method of experimental design and mathematical modeling, which can effectively reduce the number of experiments, investigate the interaction between influencing factors, and give the best condition for the experiment. In this paper, RSM design experiment using Box-Behnken Design (BBD) was used to optimize the experimental conditions for the degradation of SA by MBC activated PI. MBC dosage (A: 0.02–0.18 mg/L), PI dosage (B: 0.05–0.25 mM), pH (2–8) were variable input parameters, and SMZ dosage (10 mg/L) was constant. Table S1 lists their actual and coded values at different levels (–1, 0, and +1). The SMZ degradation rate is the corresponding output response, which is analyzed and predicted by the second-order polynomial model, as shown in Eq. (1).

$$Y = \alpha_0 + \sum_{i=1}^{n} \alpha_i X_i + \sum_{i=1}^{n} \alpha_{ii} X_i^2 + \sum_{i=1}^{n} \alpha_{ij} X_i X_j + \beta \quad (1)$$

Here, α_0, α_i, α_{ii} and α_{ij} represent the coefficients of regression; X_i and X_j are the coded independent variables; Y is the response of SMZ degradation and β is a model error (Rashtbari et al., 2023).

2.5. Characterization methods

The surface morphology of BC and MBC was detected by JEOL-SM-7401F SEM. The aperture and specific surface area of BC and MBC were characterized by BET (Quantchrome Autosorb-iQ, USA). X-ray diffraction (XRD) was performed on a Bruker D8 Advance X-ray diffractometer and the crystal structures of BC and MBC were recorded. X-ray photoelectron spectroscopy (XPS) was performed on an ESCALAB 250xi and the elemental valence state was detected. The functional groups on BC and MBC surfaces were detected using a Fourier transform infrared spectrometer (FTIR, Perkin Elmer, USA). The 5,5-dimethyl-1-pyrroline n-oxide (DMPO) and 2,2,6,6-tetramethylpiperidine (TEMP)

were used as trapping agents to identify free radicals by electron paramagnetic resonance (EPR, Bruker A300, Germany). Electrochemical experiments were carried out with the CHI760E electrochemical workstation. The soluble Mn(III) was determined by ultraviolet spectrophotometer UV2450.

3. Results and discussion

3.1. Material characterization

The surface morphology of BC and MBC is shown in Fig. 1a-d. It can be seen that the surface of the BC was rough and exhibited a micropore structure. The surface of the MBC was rougher than that of BC, and there were clumpy and spherical particles on the surface. The elemental composition of the materials were analyzed by element mapping and energy dispersive spectrometer (EDS), as shown in Fig. 1e-h. The MBC was mainly composed of C, O and Mn. These results indicated that MnO_x were successfully loaded on the surface of the BC. In addition, it can be seen from the desorption and adsorption isotherm of nitrogen that both BC and MBC have abundant pore structures (Fig. S1). The BET-specific surface area (Table S2) of BC and MBC were 37.9 m^2/g and 127.3 m^2/g, respectively, and the pore volume increased from 0.052 cm^3/g to 0.177 cm^3/g. The loading of MnO_x caused a substantial increase in pore volume and surface area (Li et al., 2018, Tan et al., 2022).

The structures of BC and MBC samples were confirmed by XRD analysis (Fig. S2). The peak at 26.70° corresponds to the crystal surface (002) of BC (Gong et al., 2024). After modification, additional diffractions indexed as (002), (-111) and (-113) planes appeared at 28.126°, 36.572° and 50.314°, which matched with the standard card JCPDS No. 31–1048 of K_xMnO_2. In comparison to BC, the diffraction peak intensity of MBC at 20.845°, 28.695°, 34.496°, and 50.112° was lower. This is because the supported manganese reduced the diffraction peak intensity of other crystals (Escande et al., 2015).

Fig. 2a shows the XPS survey spectrum of BC and MBC. The MBC showed a new characteristic peak with the binding energy of 642.30 eV, representing for Mn. The peak C-O and C═O peaks (at 285.88 and 289.38 eV respectively) were enhanced, while π-π* satellite peaks disappeared after loading MnO_x, as shown in Fig. 2b. The O1s of BC can be fitted to three sub-peaks of 532.48 eV, 531.58 eV, and 530.68 eV, representing the vibration of C═O, C-O, and O-H, respectively (Dai et al., 2017, Wang et al., 2017). Similarly, after loading MnO_x, the peak became wider and the ratio of C═O increased. MBC exhibited a new characteristic peak at a binding energy of 529.04 eV, corresponding to the Mn-O group (Mian et al., 2019, Song et al., 2014). From Fig. 2d, it can be seen that manganese was predominantly Mn(IV) and contained some Mn(II). Mn(III) was difficult to discriminate due to the proximity of its binding energy to divalent Mn(II).

The FTIR analysis of the samples are shown in Fig. S3. The peaks at 3430.2 cm^{-1}, 1586.4 cm^{-1}, 1392.2 cm^{-1}, 1087.1 cm^{-1}, 792.6 cm^{-1} were attributed to hydroxyl (–OH), C═O, C–H, C–O, and C–C stretching vibrations, respectively (Tang et al., 2015, Xu et al., 2014). These functional groups have the potential to enhance substance adsorption and improve the efficiency of PI activation. After loading MnO_x, the hydroxyl peak shifted to 3400.3 cm^{-1}. It seemed that there was an

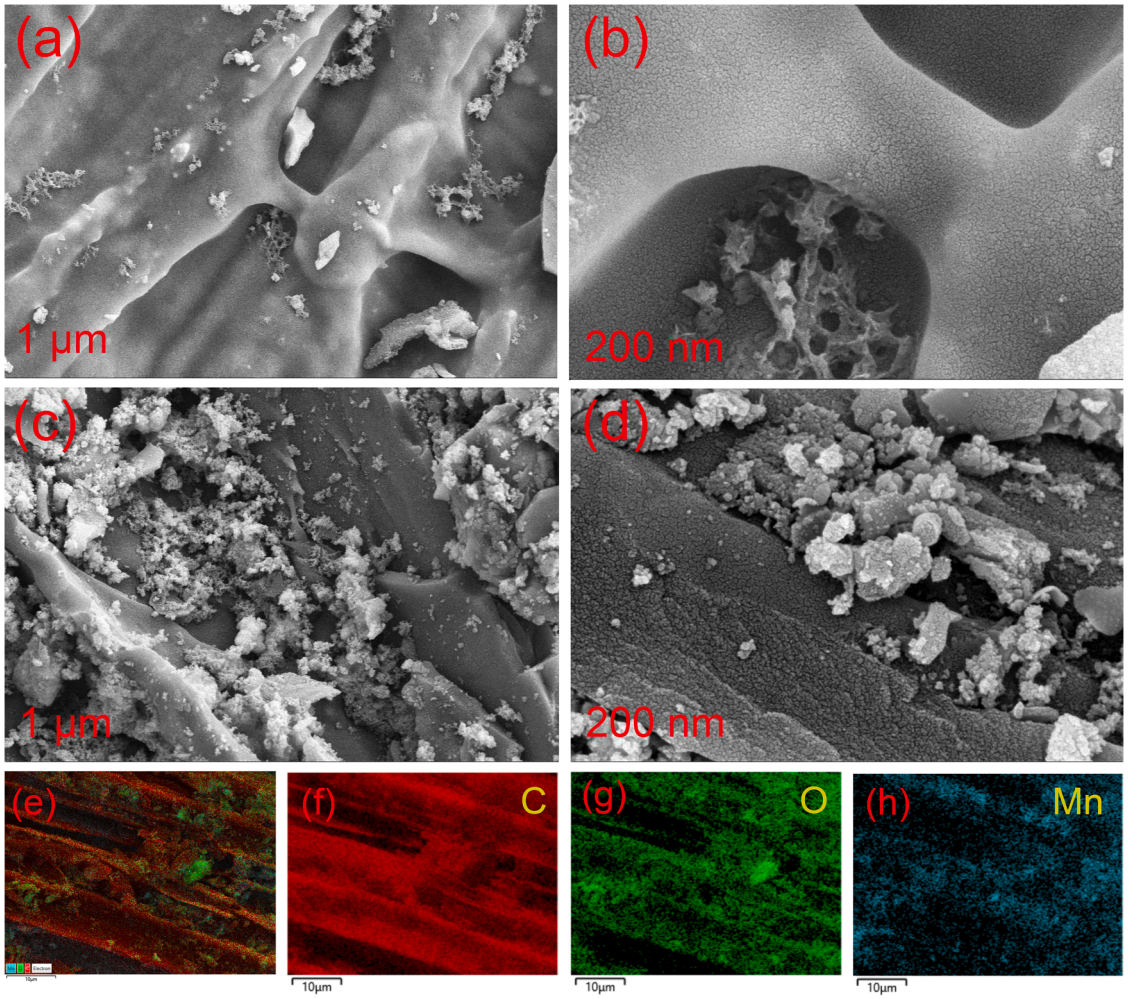

Fig. 1. SEM images of BC (a, b) and MBC (c, d); EDS images of MBC (e-h).

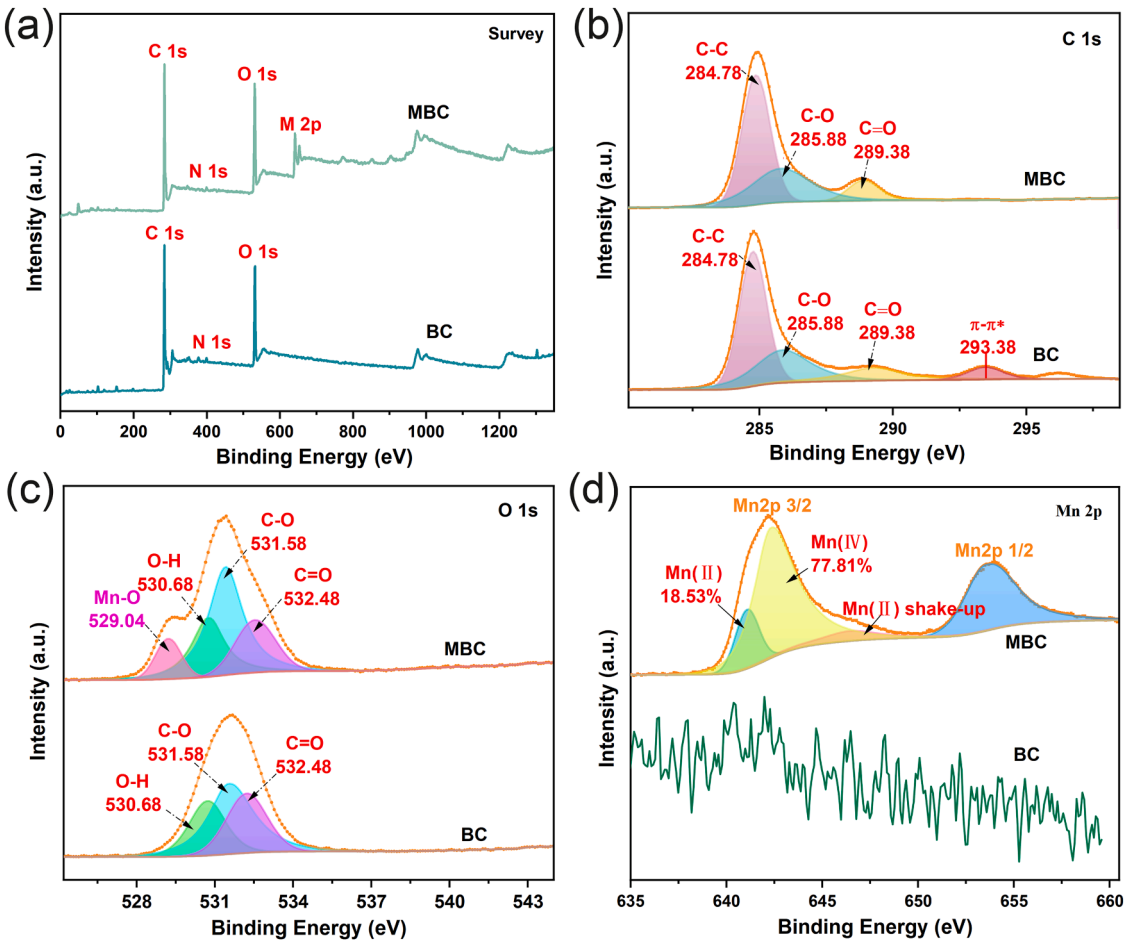

Fig. 2. XPS spectra of BC and MBC: survey spectra (a), C1s (b), O1s (c), Mn 2p (d).

interaction between the surface –OH and MnO_x (Kadimpati et al., 2024), which could enhance the electron trapping ability of the catalysts (Li et al., 2021). The peak densities of C═O and C–O were significantly increased, consistent with the XPS characterization results. This indicates the introduction of numerous oxygen-containing groups by MnO_x, enhancing the hydrophilicity of the material surface and facilitating the adsorption of organic compounds (Tang et al., 2023). New characteristic peaks appeared in MBC near 519.5 cm^{-1} and 758.5 cm^{-1}, which was attributed to the formation of Mn–O (Hsu et al., 2014), and the exposure of metal oxide sites would benefit catalytic reactions (Zhou et al., 2021).

3.2. Catalytic effect of MBC/PI system

The results of SMZ degradation by BC, MnO_2, and MBC catalyzed PI are shown in Fig. 3a. The degradation effect of the MBC/PI system was significantly better than that of the other two systems. The SMZ removal rate of the MBC/PI system reached 98.2 % after a 30 minute reaction, which was significantly higher than that of the MnO_2/PI system (75.2 %) and BC/PI system (32.2 %). The degradation process conformed to the pesudo-first-order kinetic model, as shown in Fig. 3a. The pesudo-first-order kinetic rates of MBC degradation (K_{obs}) in the MBC/PI system were much larger than those in the BC/PI and MnO_2/PI systems.

The influence of MBC amount on the degradation of SMZ is shown in Fig. S4(a). The degradation rate showed a trend of first increasing and then decreasing with the increase of MBC addition from 0 g/L to 0.4 g/L. The initial increase was because MBC provided more active sites. When MBC was added more, the active sites were masked, resulting in the weakening of the PI activation. In addition, excessive catalyst may lead to ROS loss, thus weakening the degradation effect on SMZ (He et al., 2021a, 2021b). In brief, the optimal dosage of MBC was 0.1 g/L. The effect of PI concentration on the degradation of SMZ in the MBC/PI system is shown in Fig. S4(b). With the increase in PI concentration, the SMZ degradation rate showed an increasing trend. In control without PI in solution, the SMZ concentration did not decrease significantly, indicating that the adsorption of SMZ on MBC was negligible. The increase in SMZ degradation rate was not obvious when the PI concentration exceeded 0.15 mM, which might be attributed to the limitation of MBC active site (He et al., 2021a, 2021b).

pH plays a crucial role in the oxidation process (He et al., 2022a, 2022b). It can be seen from Fig. S4(c) that SMZ was degraded significantly in the wide pH range of 2–7, and pH 5 was the optimal condition. The SMZ degradation rate decreased when pH > 9 and was only 15 % at pH 12. The point of zero charge (pHpzc) of MBC was determined to be 2.45, as shown in Fig. S5. When pH > 2.45, the surface of MBC is negatively charged. When pH > 9, a stronger repulsion existed between the MBC surface and the periodate anion, blocking the contact between PI and the active sites on the surface of the MBC and limiting the reaction rate (Ahmad and Ansari, 2021, Panahi et al., 2020). At lower pH (pH < 5), the acidic environment reduced the amount of dissociated PI in the form of anions, thus slightly reducing the activation efficiency (Guan et al., 2011).

The common inorganic anions are one of the most important influence factor on the degradation reactions. Therefore, the effects of inorganic anions (Cl^-, HCO_3^-, $H_2PO_4^-$, NO_3^-, SO_4^{2-}) were investigated, as shown in Fig. 3b and Fig. S6. HCO_3^- and $H_2PO_4^-$ had slight inhibition on SMZ degradation. The inhibitory effect of HCO_3^- might be due to two factors. One was that HCO_3^- changed pH of the reaction system, and the

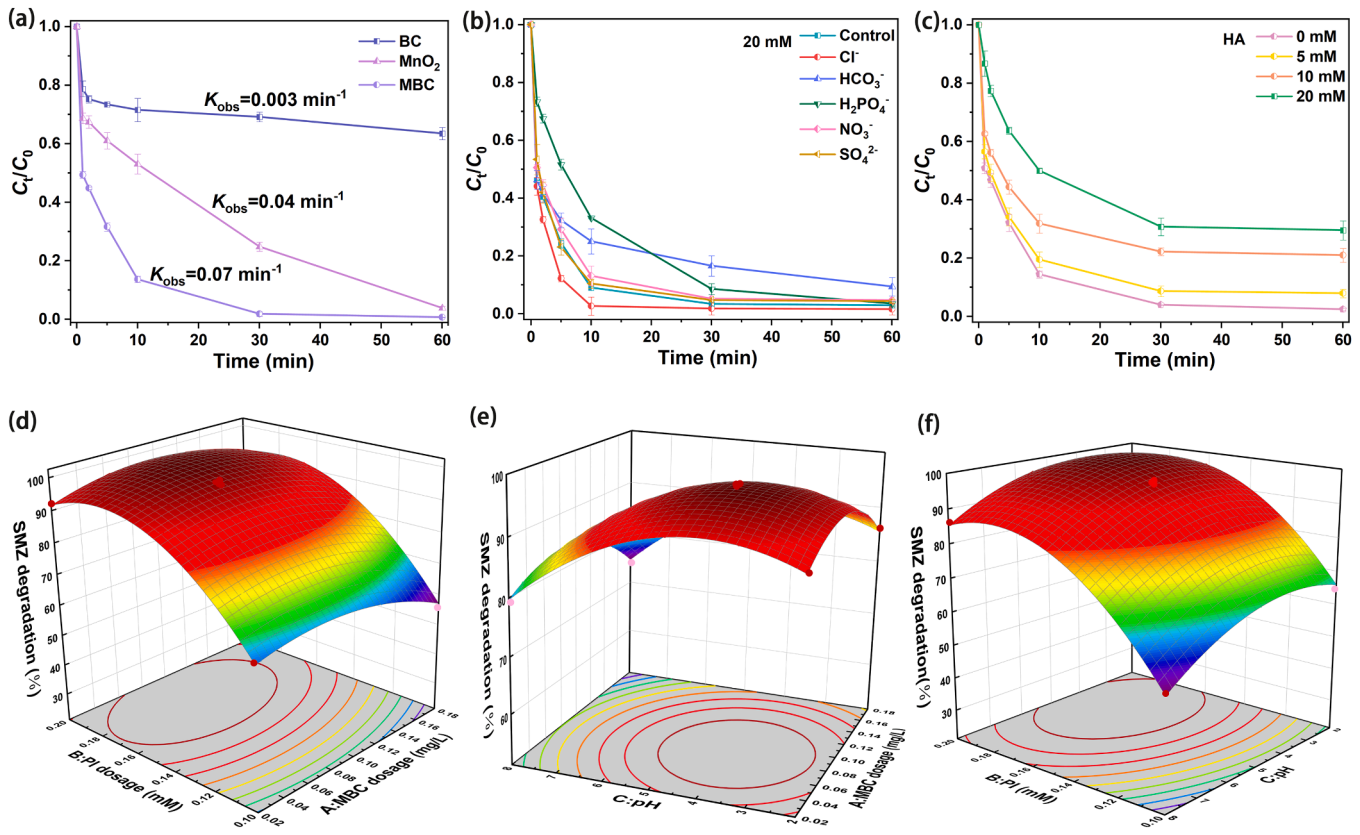

Fig. 3. The removal efficiency of SMZ and the first-order kinetic fitting K_{obs} in BC, MnO_2, and MBC activated PI systems (a), anion species (20 mM) (b) and HA (c) on the degradation. 3D response surface plot showing the interaction between MBC dosage and PI dosage (d), MBC dosage and pH (e)) and PI dosage and pH (f) for SMZ degradation. Default reaction conditions: [SMZ] = 10 mg/L, [PI] = 0.15 mM, [MBC] = 0.1 g/L, pH 5, 25°C.

other was that HCO_3^- consumed free radicals in the system (Rafiei et al., 2021). $H_2PO_4^-$ inhibited catalytic activity by attaching to the surface of catalyst and formed an inner-circle compound with MnO_x, which inhibited the role of MnO_x (Li et al., 2023a, 2023b). In the presence of Cl^-, NO_3^-, and SO_4^{2-}, the SMZ degradation rate was virtually unaffected. Overall, the MBC/PI system degraded SMZ with slight interference from anions. Furthermore, the effect of HA, one of the common dissolved organic matter (DOM), on the reactions was investigated. Fig. 3c indicated HA had an inhibitory effect on SMZ degradation, and the inhibition was enhanced with increasing HA concentration. This can be attributed to that HA adsorbed on the surface of MBC occupied the active sites of PI, and consumed the active species in the reaction system (Xie et al., 2024, Zhu et al., 2022).

3.3. Multiple statistical analysis

The BBD design matrix with SMZ degradation rate as response, and MBC dosage, PI dosage and pH as influencing factors is shown in Table S3. The polynomial quadratic model equation (Eq. (2)) could give the interaction between the independent input variable and the predicted output response.

$$Y = 96.40 - 2.34A + 14.94B - 5.28C + 1.72AB - 0.2AC + 1.1BC - 6.24A^2 - 14.19B^2 - 7.76C^2 \quad (2)$$

Here, A (SMZ dosage), B (PI dosage), and C (pH) are the coded units and Y is the response of SMZ degradation.

The variance analysis of the model is shown in Table S4. The F-value of the model is 133.99 and the *p*-value is less than 0.0001, indicating that there is a significant correlation between SMZ degradation rate and the input variables. The R^2 value of the model is 0.994 and the adjusted R^2 value is 0.987, verifying the accuracy of the model. In addition, the signal-to-noise ratio is an adequate measure of accuracy and requires greater than 4. The signal-to-noise ratio of this model is 33.32, indicating that it was fully accurate. The coefficient of variation of 2.04 (< 10) indicates that the model has good repeatability (Jawad and Surip, 2022). All the above data indicate that the model is accurate, reliable and repeatable for predicting SMZ degradation rate using MBC dose, PI dose and pH. The relationship between the F-values of the three factors is as B>C>A. Since F-value can indicate the influence degree of factors on the response, PI dose has the greatest influence on SMZ degradation rate among the three factors, followed by pH and MBC dose.

Fig. S7(a) is a diagram showing the test for the normality of the residual. In this figure, there is no deviation in the normality of the residual. The data obtained by the model is almost distributed on a straight line, few points deviate from the line, with R^2 of 0.994. This indicates that the normality of the residual is acceptable. The predicted degradation rates of SMZ is very close to the actual ones (Fig. S7(b)).

Fig. 3(d), (e), and (f) are the pairwise interaction response surface diagrams of the effects of MBC dose, PI dose and pH on SMZ degradation rate. As can be seen from the figures, when MBC dose and PI dose with each other to affect SMZ degradation rate, the response surface gradient is more inclined than that of the other two groups. In addition, contour shapes are more elliptical. Since the response surface gradient and contour shape can well describe the intensity of the interaction, the larger the gradient, and the closer the contour shape to ellipse, the stronger the interaction. Therefore, among the three influencing factors in this experiment, MBC dose and PI dose have the strongest interaction. The optimal conditions for SMZ degradation predicted by this model are 0.12 mg/L of MBC, 0.17 mM PI, and pH 3.5.

3.4. Oxidizing reactive species and electrochemical analysis

Quenching experiments and EPR analysis were carried out to characterize the ROS species in the MBC/PI-catalyzed SMZ degradation systems. FFA and L-His were selected as quenchers of $^1O_2$, phenol as a quencher of IO_3•, MeOH and TBA as scavengers of •OH, and CF was utilized to quench the O_2•$^-$ (Sun et al., 2019, Wenyu et al., 2013, Yao et al., 2016). The results are shown in Fig. 4a. SMZ degradation rate was almost unaffected in the presence of TBA and CF. Addition of phenol, L-His, and FFA significantly inhibited the removal of SMZ, and the degradation rate decreased from 96.6 % to 6.5 %, 5.0 %, and 64.6 %, respectively. The presence of MeOH slightly inhibited the reaction and the SMZ degradation rate was reduced from 96.6 % to 89.3 %. This indicated that IO_3• and $^1O_2$ played a major role in the MBC/PI system, followed by a small amount of •OH. To further verify the results of the quenching experiments, EPR analysis was carried out using DMPO and TEMP as trapping agents. As shown in Fig. 4b-d, DMPO-•OH (1:2:2:1), DMPO-O_2•$^-$ (1:1:1:1:1:1:1:1), and TEMP-$^1O_2$ (1:1:1) signals were detected. The signal of TEMP-$^1O_2$ peak was much stronger than that of DMPO-•OH and DMPO-O_2•$^-$. All the results indicated that the primary active species during the reaction were IO_3• and $^1O_2$, while •OH had a supporting role. The O_2•$^-$ played a negligible part.

Electrochemical analyses were performed to evaluate the electron transfer process during the reaction. It is evident from the

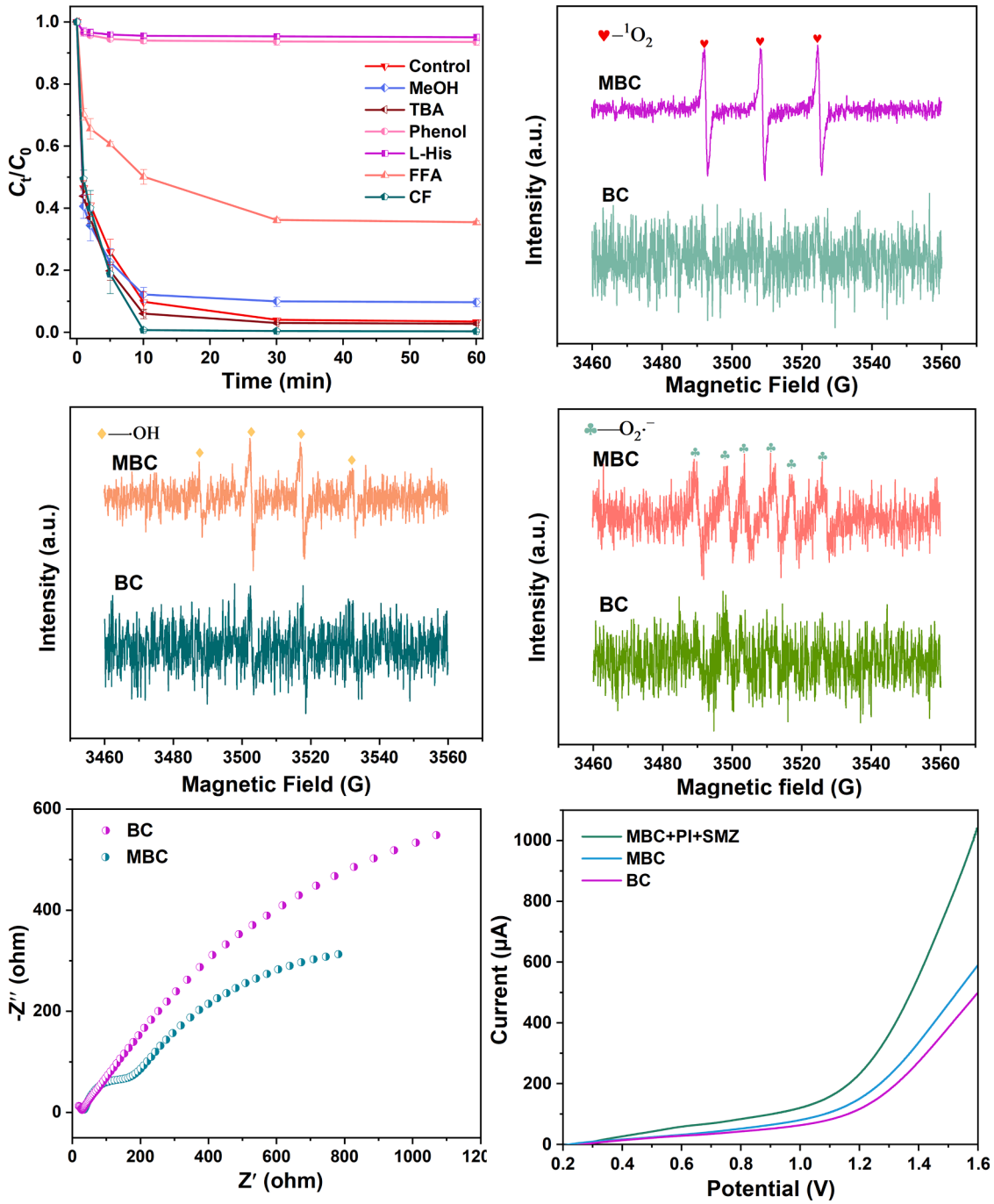

Fig. 4. Oxidation experiment using different quenchers (a); EPR signals of TEMP-$^1O_2$ (b), DMPO-•OH (c), and DMPO-O_2•$^-$ (d); electrochemical impedance spectroscopy (EIS) (e) and linear voltammetric scan (LSV) (f) plots of BC and MBC. Default experimental conditions: [SMZ] = 10 mg/L, [PI] = 0.15 mM, [MBC] = 0.1 g/L, [Quencher] = 15 mM, pH 5, 25°C.

electrochemical impedance (EIS) analysis (Fig. 4e) that MBC had a lower charge transfer resistance due to its reduced half-arc diameter (Seo et al., 2024). The current changes of the MBC-modified electrodes were measured using linear voltammetric scanning (LSV). The current response of the three different systems, BC, MBC, and MBC+PI+SMZ, are shown in Fig. 4f. The MBC+PI+SMZ system's oxidation current was shown to be much larger than that of the other two systems. This observation implied that a strong electron transfer took place following the addition of SMZ.

3.5. Analysis on activation process

The above experimental results indicated that IO_3•, $^1O_2$, and •OH were the main ROS in the MBC/PI oxidation system. XPS characterization of MBC before and after the reaction was carried out, and the XPS spectrum of Mn2p was shown in Fig. 5a. The results indicated a slight change in the valence state of Mn, with an increase in Mn(IV) and a decrease in Mn(II). The dissolved Mn(III) were detected, as shown in Fig. 5b. The characteristic peak of Mn(III)-PP complex appeared at the absorbance of 258 nm in MBC+PI+SMZ system (Wang et al., 2024), indicating the presence of dissolved Mn(III). The dissolved Mn(III) had strong oxidation and was prone to disproportionation to form Mn(IV) and Mn(II). During the disproportionation process, a high oxidation reduction potential was produced and it was easy to degrade organics (Zhang et al., 2023). The above results revealed three activation mechanisms. The first one was the role of Mn. As shown in XPS spectrum (Fig. 5a), the ratio of Mn(II) decreased and that of Mn(IV) increased after oxidation reaction. The Mn(II) reacted with periodate ions to produce $MnO(OH)_2$ and O_2•$^-$ (Eq. (3)) (Wang et al., 2012). $MnO(OH)_2$ then proceeded with O_2•$^-$ and periodate ions to generate $^1O_2$ and Mn(III) (Eq. (4)). Mn(II) reacted with O_2•$^-$ to form Mn(III) (Eq. (5)), immediately followed by disproportionation of Mn(III) to form Mn(II) and Mn(IV) (Eq. (6)–(7)) (Qian et al., 2019). In addition, $^1O_2$ acted as an active species to attack SMZ and H_2O_2 was generated in this process (Eq. (8)) (Zhong and Zhang, 2019). The redox cycling Mn(II)/Mn(III) and Mn (III)/Mn(IV) are the key to the production of IO_3•, $^1O_2$, and •OH in PI activate. In addation the generated Mn(III) was strongly oxidizing and could oxidatively degrade SMZ. In the MnO_2/bisulfite (BS) system, the dissolved Mn(III) generated is directly involved in the oxidation of bisphenol A (BPA) (Zhou et al., 2022). This mechanism is rarely revealed in the advanced oxidation process dominated by PI. The second was the role of MBC. The oxygen-containing functional groups on MBC surface provided electrons and became activation sites to produce $^1O_2$, IO_3•, and •OH (Eqs. (9)-(10)) (Chen et al., 2018, Wang et al., 2019). BET and XPS results showed that loading MnO_x increased the surface area of MBC and the surface oxygen content, which enhanced the activation of BC and the

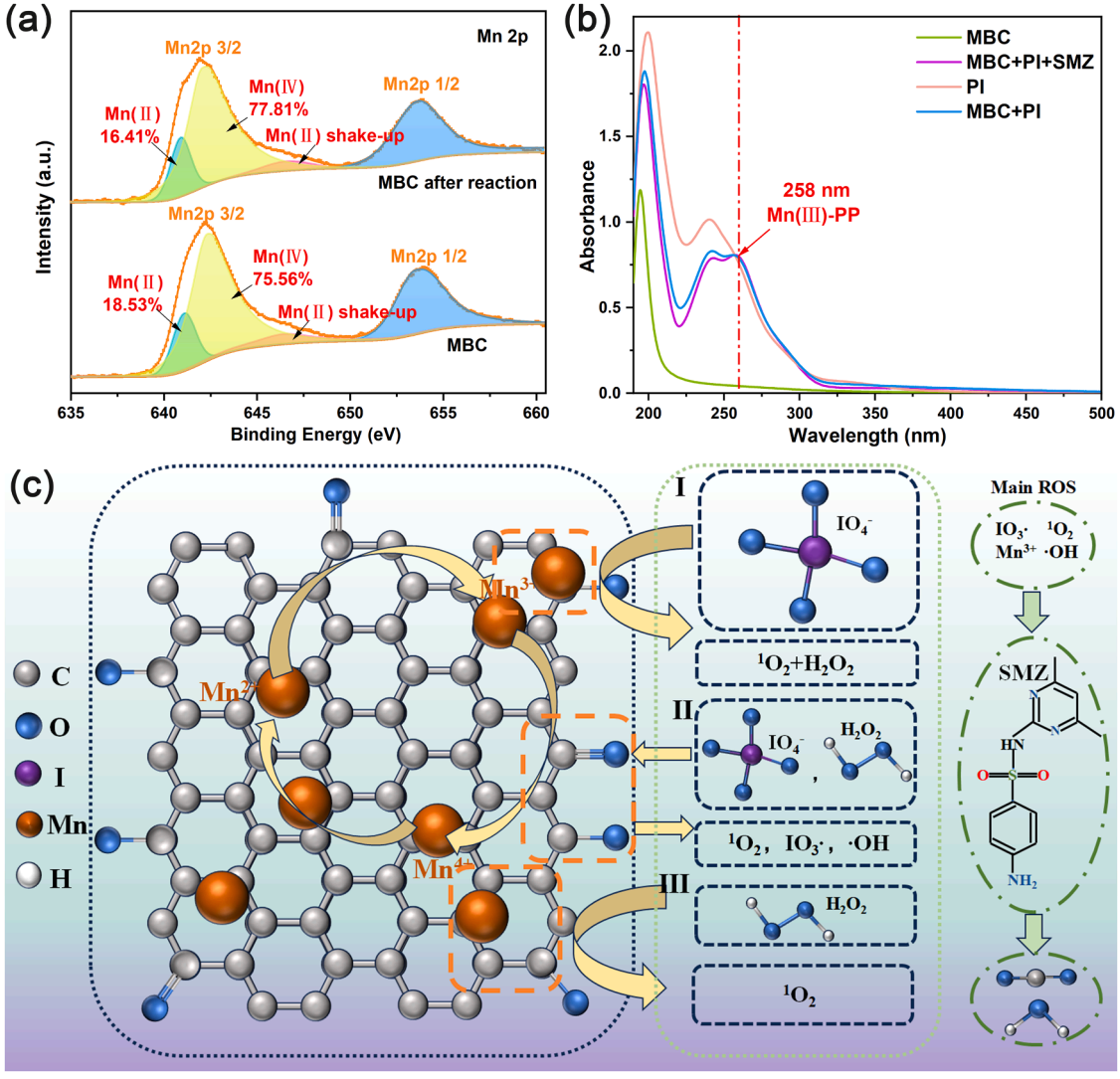

Fig. 5. XPS spectra of Mn before and after the reaction (a), wavelength scan of the reaction solution by UV–visible spectrophotometer (b), mechanism of SMZ degradation by MBC/PI-activated PI (c).

electron transfer. The FTIR of MBC (Fig. S3) showed the presence of C-O, C═O, and O-H in the sample, and these oxygen-containing functional groups produced $^1O_2$, IO_3•, and •OH in the presence of PI (Xiao et al., 2022).The third was the combined effect of MBC and Mn, where Mn(II) combined with C-O on the BC surface to form BC-O- Mn(II), which could react with H_2O_2 to produce active species (Zhang et al., 2021) (Eq. (12)). The complete mechanism was briefly depicted in Fig. 5c.

$$Mn(II) + 2IO_4^- + O_2 + 3H_2O \rightarrow MnO(OH)_2 + 2IO_3^- + 4H^+ + 2O_2\bullet^- \quad (3)$$

$$MnO(OH)_2 + IO_4^- \rightarrow MnO(OH) + IO_3^- + {}^1O_2 + H^+ \quad (4)$$

$$O_2\bullet^- + Mn(II) + 2H^+ \rightarrow Mn(III) + H_2O_2 \quad (5)$$

$$Mn(III) + e^- \rightarrow Mn(II) \quad (6)$$

$$2Mn(III) + 2H_2O \rightarrow Mn(IV) + Mn(II) + 4H^+ \quad (7)$$

$$2O_2\bullet^- + 2H_2O \rightarrow {}^1O_2 + H_2O_2 + 2OH^- \quad (8)$$

$$BC\text{-}C{=}O + H_2O_2 \rightarrow BC\text{-}C + {}^1O_2 + H_2O \quad (9)$$

$$BC\text{-}C\text{-}O + H_2O_2 \rightarrow BC\text{-}C + {}^1O_2 + H_2O \quad (10)$$

$$BC\text{-}OH + IO_4^- \rightarrow BC\text{-}O + IO_3\bullet + \bullet OH \quad (11)$$

$$BC\text{-}O\text{-}Mn(IV) + H_2O_2 \rightarrow BC\text{-}Mn(IV) + {}^1O_2 + H_2O \quad (12)$$

3.6. SMZ degradation pathway speculation

To investigate the possible degradation pathways of SMZ, the intermediate products were characterized using HPLC-MS. The mass spectra and the structures of the intermediate products are shown in Fig. S8 and Table S2. Based on the structures of the products, four possible transformation pathways of SMZ were proposed, as shown in Fig. 6. (1) P1 (*m/z* 215) was generated by Smiles-type rearrangement and SO_2 extrusion, and then amino group on the benzene ring was oxidized to hydroxyl to generate P2 (*m/z* 216), while partial P1 was transformed to P7 (*m/z* 227) under the action of ROS. P2 was then further oxidized to generate P3 (*m/z* 110) or P4 (*m/z* 124). (2) The oxidation of the amine group led to the production of P5 (*m/z* 309). Then P5 released SO_2 to produce P6 (*m/z* 245), followed by S-N bond of P6 breaking to produce P7. (3) SMZ may undergo S-C bond breaking in the presence of ROS and Mn^{3+} to produce the product P8 (*m/z* 202), and finally the benzene ring was opened to produce P9 (*m/z* 113). (4) The sulfonamide bond S-N was attacked by ROS as well as Mn^{3+} to break to generate P4 (*m/z* 124), which continued to generate P10 (*m/z* 140). Eventually, parts of the above intermediates will be mineralized into CO_2, H_2O, and some other inorganic small molecule compounds.

3.7. Stability of MBC

Furthermore, the stability of MBC was evaluated, and the results are shown in Fig. 7a. Under the same experimental conditions, five cycles were set up, and the degradation rate of SMZ could still reach 80 % after the fifth cycle. These indicated that MBC had strong catalytic stability in the MBC/PI oxidation system. A reason for the decrease in SMZ degradation rate after several cycles might be the loss of MBC during the filtration process. Combining XPS and FTIR analysis, as shown in Fig. 7b–c, the elemental species and functional groups on the surface of MBC were almost unchanged after cycling for four times, which also indicated that MBC had a good stability.

4. Conclusion

In this study, the BC material loaded with MnO_x was synthesized by the impregnation method to activate PI and oxidize SMZ. The MBC/PI system had a much better oxidation efficiency than sole MnO_2 or BC activation systems, and had a wide pH application range. The optimal experimental conditions for the removal of 10 mg/L SMZ by MBC/PI system were MBC dosage of 0.1 g/L, PI concentration of 0.15 mM and pH 5. MBC reacted with PI to produce active species IO_3•, $^1O_2$, and •OH, in which IO_3• and $^1O_2$ played critical roles. Dissolved Mn(III) was also detected in the oxidation system. Loading of MnO_x enhanced electron transfer between BC and PI, which was also an important oxidative mechanism. The transformation process of reactive species was

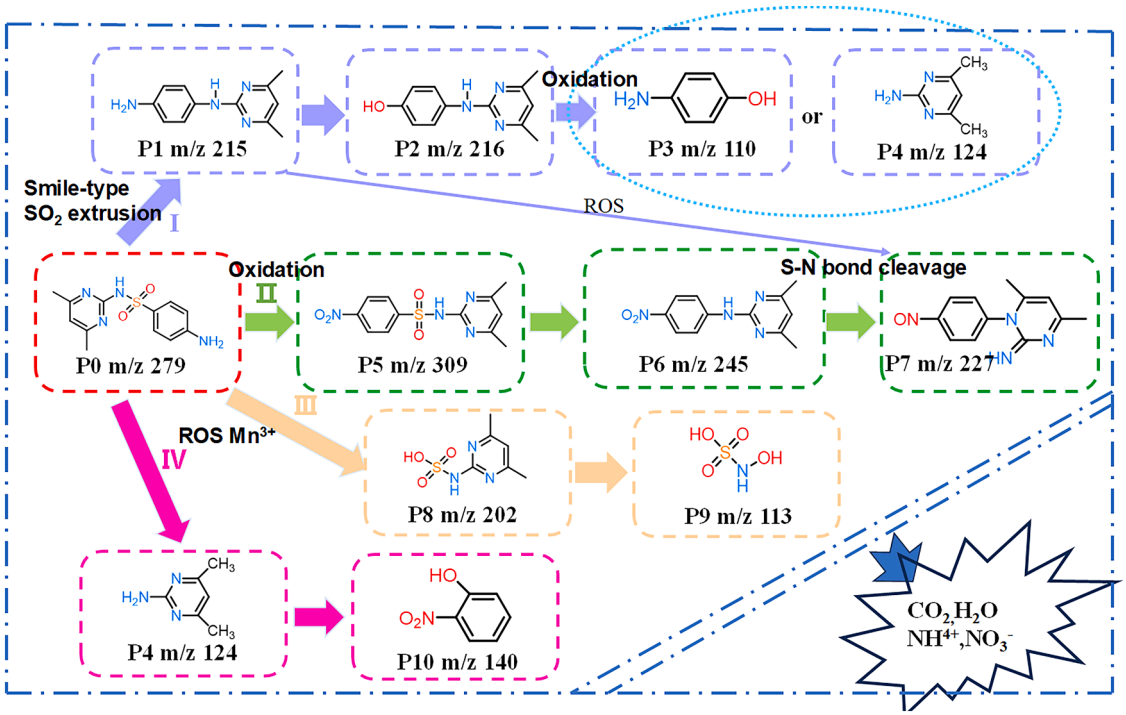

Fig. 6. Possible SMZ degradation pathways.

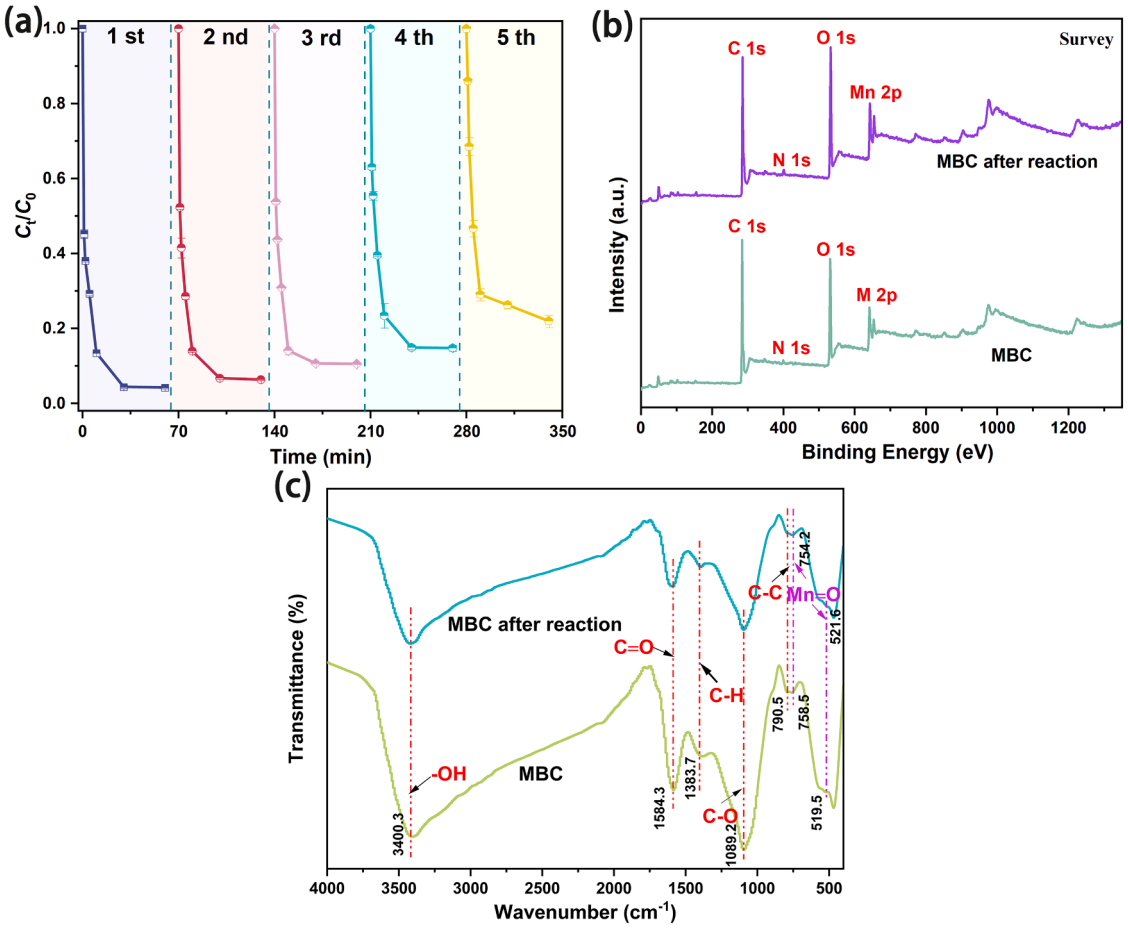

Fig. 7. Cyclic test for degradation of SMZ by MBC/PI system (a); XPS survey (b) and FTIR spectra of MBC before and after reaction (c). Default reaction conditions: [SMZ] = 10 mg/L, [PI] = 0.15 mM, [MBC] = 0.1 g/L, pH 5, 25°C.

deduced. The manganese redox cycles, abundant oxygen-containing functional groups on biochar surface, and BC-O-Mn(II) complex were involved in reactive species production. Four degradation pathways of SMZ were proposed, namely, smile-type rearrangement and SO_2 extrusion, amine-based oxidation, S-C bond breaking and sulfonamide bond S-N breaking, respectively. MBC could be reused for three times, with no obvious morphology change. This study provides both theoretical and applied value for removal of SA with MBC activated periodate technology.

CRediT authorship contribution statement

Hao Lu: Supervision, Methodology, Investigation, Data curation. **Wenyi Xie:** Investigation, Data curation. **Yang Guo:** Investigation, Data curation. **Zimu Xu:** Investigation. **Jiaqi Shi:** Writing – review & editing, Resources, Project administration, Methodology, Formal analysis, Data curation, Conceptualization. **Shaohua Cao:** Investigation, Data curation. **Xin Zhu:** Investigation. **Shuheng Hu:** Writing – review & editing, Writing – original draft, Methodology, Investigation, Data curation, Conceptualization. **Han Gao:** Supervision, Methodology, Formal analysis, Data curation, Conceptualization.

Declaration of Competing Interest

The authors declare that they have no known competing financial interests or personal relationships that could have appeared to influence the work reported in this paper.

Acknowledgements

This work was supported by the National Key Research and Development Program of China (2023YFC3706000), National Natural Science Foundation of China (No. 21707041), the Innovative Team Project of Nanjing Institute of Environmental Sciences, MEE (ZX2023QT012), Integration of Ecological and Environmental Protection in Yangtze River Delta Program of Nanjing Institute of Environmental Sciences, MEE (ZX2022QT047), and the Anhui Institute of Ecological Civilization (AHSWY-2023–1, AHSWY-2023–2).

Appendix A. Supporting information

Supplementary data associated with this article can be found in the online version at doi:10.1016/j.ecoenv.2025.117700.

Data availability

Data will be made available on request.

References

Ahmad, R., Ansari, K., 2021. Comparative study for adsorption of congo red and methylene blue dye on chitosan modified hybrid nanocomposite. Process Biochem 108, 90–102. https://doi.org/10.1016/j.procbio.2021.05.013.

Anjali, R., Shanthakumar, S., 2019. Insights on the current status of occurrence and removal of antibiotics in wastewater by advanced oxidation processes. J. Environ. Manag. 246, 51–62. https://doi.org/10.1016/j.jenvman.2019.05.090.

Baran, W., Adamek, E., Ziemianska, J., Sobczak, A., 2011. Effects of the presence of sulfonamides in the environment and their influence on human health. J. Hazard. Mater. 196, 1–15. https://doi.org/10.1016/j.jhazmat.2011.08.082.

Binh, V.N., Dang, N., Anh, N.T.K., Ky, L.X., Thai, P.K., 2018. Antibiotics in the aquatic environment of Vietnam: sources, concentrations, risk and control strategy. Chemosphere 197, 438–450. https://doi.org/10.1016/j.chemosphere.2018.01.061.

Champagne-Jorgensen, K., Kunze, W.A., Forsythe, P., Bienenstock, J., Neufeld, K.A.M., 2019. Antibiotics and the nervous system: more than just the microbes? Brain Behav. Immun. 77, 7–15. https://doi.org/10.1016/j.bbi.2018.12.014.

Chen, L.W., Yang, S.J., Zuo, X., Huang, Y., Cai, T.M., Ding, D.H., 2018. Biochar modification significantly promotes the activity of Co_3O_4 towards heterogeneous activation of peroxymonosulfate. Chem. Eng. J. 354, 856–865. https://doi.org/10.1016/j.cej.2018.08.098.

Chen, S., Zhang, W., Li, J.Y., Yuan, M.Z., Zhang, J.H., Xu, F., Xu, H.T., Zheng, X.Y., Wang, L.Q., 2020. Ecotoxicological effects of sulfonamides and fluoroquinolones and their removal by a green alga *(Chlorella vulgaris)* and a cyanobacterium *(Chrysosporum ovalisporum)*. Environ. Pollut. 263, 114554. https://doi.org/10.1016/j.envpol.2020.114554.

Cuerda-Correa, E.M., Alexandre-Franco, M.F., Fernández-González, C., 2020. Advanced oxidation processes for the removal of antibiotics from water. An overview. Water 12, 102. https://doi.org/10.3390/w12010102.

Dai, J., Wang, Z.Q., Zhu, A.X., Ji, Y.F., Kong, Z., Cai, T.M., Ding, D.H., 2023. Elimination of sulfadiazine and its metabolite from hydrolyzed urine by biochar activated periodate process: Lower environmental risk compared with $CoFe_2O_4$/peroxymonosulfate process. Chem. Eng. J. 472, 145080. https://doi.org/10.1016/j.cej.2023.145080.

Dai, X.H., Xu, Y., Dong, B., 2017. Effect of the micron-sized silica particles (MSSP) on biogas conversion of sewage sludge. Water Res 115, 220–228. https://doi.org/10.1016/j.watres.2017.02.064.

Du, J.K., Xiao, G.F., Xi, Y.X., Zhu, X.W., Su, F., Kim, S.H., 2020. Periodate activation with manganese oxides for sulfanilamide degradation. Water Res 169, 115278. https://doi.org/10.1016/j.watres.2019.115278.

Escande, V., Petit, E., Garoux, L., Boulanger, C., Grison, C., 2015. Switchable alkene epoxidation/oxidative cleavage with H_2O_2/$NaHCO_3$: efficient heterogeneous catalysis derived from biosourced eco-Mn. ACS Sustain. Chem. Eng. 3, 2704–2715. https://doi.org/10.1021/acssuschemeng.5b00561.

Fan, Z.X., Zhang, Q., Li, M., Sang, W.J., Qiu, Y., Xie, C.F.Y., 2019. Activation of persulfate by manganese oxide-modified sludge-derived biochar to degrade Orange G in aqueous solution. Env. Pollut. Bioavail. 31, 70–79. https://doi.org/10.1080/26395940.2019.1577702.

Gong, J.M., Jiang, H.H., Li, X., Cheng, H., Wang, Z.Q., Cai, J.J., Li, M.F., Wang, P., Wang, H., Hu, X., Hu, X.J., 2024. Highly efficient activation of periodate by a manganese-modified biochar to rapidly degrade methylene blue. Environ. Res. 241, 117657. https://doi.org/10.1016/j.envres.2023.117657.

Guan, Y.H., Ma, J., Li, X.C., Fang, J.Y., Chen, L.W., 2011. Influence of pH on the formation of sulfate and hydroxyl radicals in the UV/peroxymonosulfate system. Environ. Sci. Technol. 45, 9308–9314. https://doi.org/10.1021/es2017363.

He, J., Tang, J.C., Zhang, Z., Wang, L., Liu, Q.L., Liu, X.M., 2021a. Magnetic ball-milled FeS@biochar as persulfate activator for degradation of tetracycline. Chem. Eng. J. 404, 126997. https://doi.org/10.1016/j.cej.2020.126997.

He, L.Y., Lv, L.X., Pillai, S.C., Wang, H.L., Xue, J.M., Ma, Y.F., Liu, Y.L., Chen, Y.L., Wu, L., Zhang, Z.L., Yang, L., 2021b. Efficient degradation of diclofenac sodium by periodate activation using Fe/Cu bimetallic modified sewage sludge biochar/UV system. Sci. Total Environ. 783, 146974. https://doi.org/10.1016/j.scitotenv.2021.146974.

He, L.Y., Yang, S.D., Shen, S.T., Ma, Y.F., Chen, Y.L., Xue, J.M., Wang, J., Zheng, L., Wu, L., Zhang, Z.L., Yang, L., 2022b. Novel insights into the mechanism of periodate activation by heterogeneous ultrasonic-enhanced sludge biochar: relevance for efficient degradation of levofloxacin. J. Hazard. Mater. 434, 128860. https://doi.org/10.1016/j.jhazmat.2022.128860.

He, L.Y., Shi, Y., Chen, Y.L., Shen, S.T., Xue, J.M., Ma, Y.F., Zheng, L., Wu, L., Zhang, Z.L., Yang, L., 2022a. Iron-manganese oxide loaded sludge biochar as a novel periodate activator for thiacloprid efficient degradation over a wide pH range. Sep. Purif. Technol. 288, 120703. https://doi.org/10.1016/j.seppur.2022.120703.

Hsu, B.Y.W., Wang, M., Zhang, Y., Vijayaragavan, V., Wong, S.Y., Chang, A.Y.C., Bhakoo, K.K., Li, X., Wang, J., 2014. Silica-F127 nanohybrid-encapsulated manganese oxide nanoparticles for optimized T_1 magnetic resonance relaxivity. Nanoscale 6, 293–299. https://doi.org/10.1039/c3nr04378a.

Jawad, A.H., Surip, S.N., 2022. Upgrading low rank coal into mesoporous activated carbon via microwave process for methylene blue dye adsorption: Box Behnken Design and mechanism study. Diam. Relat. Mat. 127, 10. https://doi.org/10.1016/j.diamond.2022.109199.

Kadimpati, K.K., Gnida, A., Turek-Szytow, J., Hellal, M.S., Gregor, M., Matula, G., Pawlyta, M.L., Monfort, O., 2024. Design of innovative hybrid biochar prepared from marine algae and magnetite: Insights into adsorption performance and mechanism. Chem. Eng. Res. Des. 201, 218–227. https://doi.org/10.1016/j.cherd.2023.11.053.

Li, D.F.N., Pan, C., Zong, Y., Wu, D.L., Ding, Y.B., Wang, C.J., Wang, S.B., Crittenden, J. C., 2023a. Ru(III)-periodate for high performance and selective degradation of aqueous organic pollutants: important role of Ru(V) and Ru(IV). Environ. Sci. Technol. 57, 12094–12104. https://doi.org/10.1021/acs.est.3c02582.

Li, L., Zhang, Q., She, Y.C., Yu, Y.B., Hong, J.M., 2021. High-efficiency degradation of bisphenol A by heterogeneous Mn-Fe layered double oxides through peroxymonosulfate activation: performance and synergetic mechanism. Sep. Purif. Technol. 270, 14. https://doi.org/10.1016/j.seppur.2021.118770.

Li, R.N., Wang, Z.W., Zhao, X.T., Li, X., Xie, X.Y., 2018. Magnetic biochar-based manganese oxide composite for enhanced fluoroquinolone antibiotic removal from water. Environ. Sci. Pollut. Res. 25, 31136–31148. https://doi.org/10.1007/s11356-018-3064-1.

Li, S., Wu, Y.A., Zheng, H.S., Li, H.B., Zheng, Y.J., Nan, J., Ma, J., Nagarajan, D., Chang, J.S., 2023b. Antibiotics degradation by advanced oxidation process (AOPs): recent advances in ecotoxicity and antibiotic-resistance genes induction of degradation products. Chemosphere 311, 136977. https://doi.org/10.1016/j.chemosphere.2022.136977.

Li, Y.J., Qiao, X.L., Zhang, Y.N., Zhou, C.Z., Xie, H.J., Chen, J.W., 2016. Effects of halide ions on photodegradation of sulfonamide antibiotics: formation of halogenated intermediates. Water Res 102, 405–412. https://doi.org/10.1016/j.watres.2016.06.054.

Liang, J., Li, X.M., Yu, Z.G., Zeng, G.M., Luo, Y., Jiang, L.B., Yang, Z.X., Qian, Y.Y., Wu, H.P., 2017. Amorphous MnO_2 modified biochar derived from aerobically composted swine manure for adsorption of Pb(II) and Cd(II). ACS Sustain. Chem. Eng. 5, 5049–5058. https://doi.org/10.1021/acssuschemeng.7b00434.

Long, Y.K., Dai, J., Zhao, S.Y., Su, Y.P., Wang, Z.Y., Zhang, Z.T., 2021. Atomically dispersed cobalt sites on graphene as efficient periodate activators for selective organic pollutant degradation. Environ. Sci. Technol. 55, 5357–5370. https://doi.org/10.1021/acs.est.0c07794.

Luo, D., Wang, L.Y., Nan, H.Y., Cao, Y.J., Wang, H., Kumar, T.V., Wang, C.Q., 2023. Phosphorus adsorption by functionalized biochar: a review. Environ. Chem. Lett. 21, 497–524. https://doi.org/10.1007/s10311-022-01519-5.

Mian, M.M., Liu, G.J., Fu, B., Song, Y., 2019. Facile synthesis of sludge-derived MnOx-N-biochar as an efficient catalyst for peroxymonosulfate activation. Appl. Catal. B-Environ. 255, 117765. https://doi.org/10.1016/j.apcatb.2019.117765.

Panahi, H.K.S., Dehhaghi, M., Ok, Y.S., Nizami, A.S., Khoshnevisan, B., Mussatto, S.I., Aghbashlo, M., Tabatabaei, M., Lam, S.S., 2020. A comprehensive review of engineered biochar: production, characteristics, and environmental applications. J. Clean. Prod. 270, 122462. https://doi.org/10.1016/j.jclepro.2020.122462.

Qian, A., Zhang, W., Shi, C., Pan, C., Giammar, D.E., Yuan, S.H., Zhang, H.L., Wang, Z.M., 2019. Geochemical stability of dissolved Mn(III) in the presence of pyrophosphate as a model ligand: complexation and disproportionation. Environ. Sci. Technol. 53, 5768–5777. https://doi.org/10.1021/acs.est.9b00498.

Qiu, M., Liu, L., Ling, Q., Cai, Y., Yu, S., Wang, S., Fu, D., Hu, B., Wang, X., 2022. Biochar for the removal of contaminants from soil and water: a review. Biochar 4, 1–25. https://doi.org/10.1007/s42773-022-00146-1.

Rafiei, N., Fatehizadeh, A., Amin, M.M., Pourzamani, H.R., Ebrahimi, A., Taheri, E., Aminabhavi, T.M., 2021. Application of UV/chlorine processes for the DR83:1 degradation from wastewater: Effect of coexisting anions. J. Environ. Manag. 297, 9. https://doi.org/10.1016/j.jenvman.2021.113349.

Rashtbari, Y., Abazari, M., Arfaeinia, L., Gholizadeh, A., Afshin, S., Poureshgh, Y., Alipour, M., 2023. The optimization of reactive black 5 dye removal in the sono-catalytic process combined with local yellow montmorillonite and hydrogen peroxide using response surface methodology from aqueous solutions. Biomass-.-. Convers. Biorefinery. 13, 6067–6081. https://doi.org/10.1007/s13399-021-01773-7.

Seo, G., Kumar, A.V.N., Shin, W.S., 2024. Periodate activation and pH regulation using ball-milled metal-oxide-mineral-biochar composite for removal of antibiotics from contaminated water. Environ. Res. 260, 119611. https://doi.org/10.1016/j.envres.2024.119611.

Song, Z.G., Lian, F., Yu, Z.H., Zhu, L.Y., Xing, B.S., Qiu, W.W., 2014. Synthesis and characterization of a novel MnOx-loaded biochar and its adsorption properties for Cu^{2+} in aqueous solution. Chem. Eng. J. 242, 36–42. https://doi.org/10.1016/j.cej.2013.12.061.

Sun, P., Liu, H., Feng, M.B., Guo, L., Zhai, Z.C., Fang, Y.S., Zhang, X.S., Sharma, V.K., 2019. Nitrogen-sulfur co-doped industrial graphene as an efficient peroxymonosulfate activator: Singlet oxygen-dominated catalytic degradation of organic contaminants. Appl. Catal. B-Environ. 251, 335–345. https://doi.org/10.1016/j.apcatb.2019.03.085.

Tan, W.T., Zhou, H., Tang, S.F., Zeng, P., Gu, J.F., Liao, B.H., 2022. Enhancing Cd(II) adsorption on rice straw biochar by modification of iron and manganese oxides. Environ. Pollut. 300, 118899. https://doi.org/10.1016/j.envpol.2022.118899.

Tan, X.F., Liu, Y.G., Zeng, G.M., Wang, X., Hu, X.J., Gu, Y.L., Yang, Z.Z., 2015. Application of biochar for the removal of pollutants from aqueous solutions. Chemosphere 125, 70–85. https://doi.org/10.1016/j.chemosphere.2014.12.058.

Tang, J.C., Lv, H.H., Gong, Y.Y., Huang, Y., 2015. Preparation and characterization of a novel graphene/biochar composite for aqueous phenanthrene and mercury removal. Bioresour. Technol. 196, 355–363. https://doi.org/10.1016/j.biortech.2015.07.047.

Tang, J.Y., Ma, Y.F., Zeng, C.Y., Yang, L., Cui, S., Zhi, S.L., Yang, F.X., Ding, Y.Z., Zhang, K.Q., Zhang, Z.L., 2023. Fe-Al bimetallic oxides functionalized-biochar via ball milling for enhanced adsorption of tetracycline in water. Bioresour. Technol. 369, 9. https://doi.org/10.1016/j.biortech.2022.128385.

Van Boeckel, T.P., Brower, C., Gilbert, M., Grenfell, B.T., Levin, S.A., Robinson, T.P., Teillant, A., Laxminarayan, R., 2015. Global trends in antimicrobial use in food animals. Proc. Natl. Acad. Sci. U. S. A. 112, 5649–5654. https://doi.org/10.1073/pnas.1503141112.

Wang, H.Z., Guo, W.Q., Liu, B.H., Wu, Q.L., Luo, H.C., Zhao, Q., Si, Q.S., Sseguya, F., Ren, N.Q., 2019. Edge-nitrogenated biochar for efficient peroxydisulfate activation: an electron transfer mechanism. Water Res. 160, 405–414. https://doi.org/10.1016/j.watres.2019.05.059.

Wang, J.L., Zhuan, R., 2020. Degradation of antibiotics by advanced oxidation processes: an overview. Sci. Total Environ. 701, 135023. https://doi.org/10.1016/j.scitotenv.2019.135023.

Wang, M.X., Tan, W.F., Feng, X.H., Koopal, L.K., Liu, M.M., Liu, F., 2012. One-step synthesis of sea urchin-like α-MnO_2 using KIO_4 as the oxidant and its oxidation of arsenite. Mater. Lett. 77, 60–62. https://doi.org/10.1016/j.matlet.2012.03.005.

Wang, X.P., Gu, L., Zhou, P., Zhu, N.W., Li, C.X., Tao, H., Wen, H.F., Zhang, D.F., 2017. Pyrolytic temperature dependent conversion of sewage sludge to carbon catalyst and

their performance in persulfate degradation of 2-Naphthol. Chem. Eng. J. 324, 203–215. https://doi.org/10.1016/j.cej.2017.04.101.

Wang, X.X., Jones, M.R., Pan, Z.Z., Lu, X.H., Deng, Y.M., Zhu, M.Q., Wang, Z.M., 2024. Trivalent manganese in dissolved forms: occurrence, speciation, reactivity and environmental geochemical impact. Water Res 263, 122198. https://doi.org/10.1016/j.watres.2024.122198.

Wenyu, Huang, Marcello, Brigante, Feng, Wu, 2013. Assessment of the Fe(lll)-EDDS complex in fenton-like processes: from the radical formation to the degradation of bisphenol A. Environ. Sci. Technol. 47, 1952–1959. https://doi.org/10.1021/es304502y.

Xiao, P.Y., Yi, X.L., Wu, M.H., Wang, X., Zhu, S.M., Gao, B.X., Liu, Y., Zhou, H., 2022. Catalytic performance and periodate activation mechanism of anaerobic sewage sludge-derived biochar. J. Hazard. Mater. 424, 127692. https://doi.org/10.1016/j.jhazmat.2021.127692.

Xie, M.Q., Liang, M.N., Liu, C.M., Xu, Z.J., Yu, Y.K., Xu, J., You, S.H., Wang, D.Q., Rad, S., 2024. Peroxymonosulfate activation by CuMn-LDH for the degradation of bisphenol A: effect, mechanism, and pathway. Ecotoxicol. Environ. Saf. 270, 115929. https://doi.org/10.1016/j.ecoenv.2024.115929.

Xu, X.Y., Cao, X.D., Zhao, L., Sun, T.H., 2014. Comparison of sewage sludge- and pig manure-derived biochars for hydrogen sulfide removal. Chemosphere 111, 296–303. https://doi.org/10.1016/j.chemosphere.2014.04.014.

Yang, H., Liu, Y.X.Y., Zhang, Y., Liu, L., Xia, S.B., Xue, Q., 2022. Secondary pyrolysis oil-based drill-cutting ash for peroxymonosulfate/periodate activation to remove tetracycline: a comparative study. Sep. Purif. Technol. 294, 121264. https://doi.org/10.1016/j.seppur.2022.121264.

Yao, Y.J., Chen, H., Lian, C., Wei, F.Y., Zhang, D.W., Wu, G.D., Chen, B.J., Wang, S.B., 2016. Fe, Co, Ni nanocrystals encapsulated in nitrogen-doped carbon nanotubes as Fenton-like catalysts for organic pollutant removal. J. Hazard. Mater. 314, 129–139. https://doi.org/10.1016/j.jhazmat.2016.03.089.

Zhang, C., Tian, S.H., Qin, F.Z., Yu, Y.L., Huang, D.L., Duan, A.B., Zhou, C.Y., Yang, Y., Wang, W.J., Zhou, Y., Luo, H.Z., 2021. Catalyst-free activation of permanganate under visible light irradiation for sulfamethazine degradation: experiments and theoretical calculation. Water Res 194, 116915. https://doi.org/10.1016/j.watres.2021.116915.

Zhang, C., Chen, Y.Y., Chen, S.L., Guan, X.C., Zhong, Y., Yang, Q.Y., 2023. Occurrence, risk assessment, and *in vitro* and *in vivo* toxicity of antibiotics in surface water in China. Ecotox. Environ. Safe. 255, 114817. https://doi.org/10.1016/j.ecoenv.2023.114817.

Zhao, R.X., Feng, J., Liu, J., Fu, W.J., Li, X.Y., Li, B., 2019. Deciphering of microbial community and antibiotic resistance genes in activated sludge reactors under high selective pressure of different antibiotics. Water Res. 151, 388–402. https://doi.org/10.1016/j.watres.2018.12.034.

Zhong, S.F., Zhang, H.C., 2019. New insight into the reactivity of Mn(III) in bisulfite/permanganate for organic compounds oxidation: the catalytic role of bisulfite and oxygen. Water Res 148, 198–207. https://doi.org/10.1016/j.watres.2018.10.053.

Zhou, R., Liu, S., He, F.R., Ren, H.J., Han, Z.H., 2021. Alkylpolyglycoside modified MnFe2O4 with abundant oxygen vacancies boosting singlet oxygen dominated peroxymonosulfate activation for organic pollutants degradation. Chemosphere 285, 11. https://doi.org/10.1016/j.chemosphere.2021.131433.

Zhou, Y., Li, X., Chen, X., Lu, J., Zhou, Y., 2022. Dual-path oxidation of phenolic organic contaminants triggered by the β-MnO_2/bisulfite system. ACS EST Water 2, 2255–2723. https://doi.org/10.1021/acsestwater.2c00365.

Zhu, H., Guo, A., Wang, S.M., Long, Y., Fan, G.Y., Yu, X.J., 2022. Efficient tetracycline degradation via peroxymonosulfate activation by magnetic Co/N co-doped biochar: emphasizing the important role of biochar graphitization. Chem. Eng. J. 450, 138428. https://doi.org/10.1016/j.cej.2022.138428.

Zhu, S.S., Li, X.J., Kang, J., Duan, X.G., Wang, S.B., 2019. Persulfate activation on crystallographic manganese oxides: mechanism of singlet oxygen evolution for nonradical selective degradation of aqueous contaminants. Environ. Sci. Technol. 53, 307–315. https://doi.org/10.1021/acs.est.8b04669.

Zou, R.S., Yang, W.Q., Rezaei, B., Tang, K., Zhang, P.P., Andersen, H.R., Keller, S.S., Zhang, Y.F., 2024. Sustainable bioelectric activation of periodate for highly efficient micropollutant abatement. Water Res. 254, 121388. https://doi.org/10.1016/j.watres.2024.121388.